Rubin, M.B.; Rodríguez-Martínez, J.A. (2014). The effect of radial inertia on flow localization in ductile rods subjected to dynamic extension. *International Journal of Impact Engineering*. 69, pp. 157-164.

DOI: https://doi.org/10.1016/j.ijimpeng.2014.02.006

The effect of radial inertia on flow localization in ductile rods subjected to dynamic extension

MB Rubin

Faculty of Mechanical Engineering
Technion - Israel Institute of Technology
32000 Haifa, Israel
Email: mbrubin@tx.technion.ac.il

JA Rodríguez-Martínez

Department of Continuum Mechanics and Structural Analisis
University of Carlos III of Madrid
Avda. de la Universidad 30, 28911 Leganés
Madrid, Spain
Email: jarmarti@ing.uc3m.es

May 2013

Keywords: Flow localization; Linear stability analysis; Perturbation growth; Radial Inertia

Abstract

The objective of this work is to investigate the influence of radial inertia on the flow localization in ductile rods subjected to dynamic extension. Using the theory of a straight Cosserat rod which includes normal cross-sectional extension it is possible to obtain an exact solution for nonlinear uniform extension of a rigid-plastic material using a functional form of the yield stress that models the effect of the more general stress field in the necking region of the rod. Linear stability analysis of this exact nonlinear solution yields equations that generalize the formulation reported by Zhou et al. (2006) to include radial stretching and inertia. Examples show the quantitative effect of radial inertia on the stabilization of the localization process and on the determination of the expected length of fragments.

1. Introduction

The foundation of analytical investigations of necking of ductile rods was proposed by Considère (Considère 1885) who postulated the well-known load maximum criterion: *the onset of necking occurs when the increment of strain hardening becomes equal to the geometric softening in a simple tension test*. To this day Considère's criterion is used in many engineering applications to estimate the onset of necking. Straightforward application of Considère's condition provides the necking strain, which is considered as the reference variable for assessment of material ductility. More specifically, Considère's condition is based on the following assumption:

- The gauge of the specimen must be such that the elongation of the neck is small in comparison with the uniform elongation which occurs before localization.
- The material is strain rate and temperature insensitive.
- The material is tested under quasi-static conditions.

The latter restriction is related to the fact that the well-established concepts of ductile failure under static loading no longer apply in the dynamic regime. At high strain rates, necking and failure are delayed by the influence of the inertia. This was the conclusion of Fyfe and Rajendran (1980) who performed a series of quasi-static and dynamic tests on different metals and observed that fracture was inhibited at high strain-rates. More specifically, these authors (Fyfe and Rajendran 1980, Rajendran and Fyfe 1982) incorporated inertia terms in the theory of plastic instability and obtained results consistent with their experimental observations. Further insight into the role played by inertia in dynamic failure of ductile materials was provided by Grady (1982). He explicitly stated that the global continuum laws used to predict dynamic failure must

include the effects of inertia. More specifically, in the closure of his work Grady (1982) claimed that "*material ductility as a phenomenon driven by local inertia forces*" needed additional investigation. This gave rise to extensive research in the field of dynamic ductile failure using experimental, computational and analytical methods.

Experimental work: Most of the experimental work is based on radial expansion of axially symmetric structures like rings (e.g. Grady and Benson, 1983; Gourdin, 1989; Altynova et al., 1996; Grady and Olsen, 2003; Zhang and Ravi-Chandar, 2006; Janiszewski, 2012), tubes (e.g. Goto et al., 2008; Hiroe et al., 2008; Zhang and Ravi-Chandar, 2010) and hemispheres (e.g. Juanicotena, 1998; Mercier et al., 2010). The symmetry of these structures nearly eliminates the effects of wave propagation before the onset of necking, which facilitates the interpretation of the experimental findings. Within the typical range of expansion velocities attained in these tests – from 50 to 300 m/s – the experimental results show that, without exception, the strain to failure of ductile materials is enhanced by the loading rate.

Computational work: Knoche and Needleman (1993) used finite element (FE) simulations to evaluate the influence of inertia on failure initiation in the round bar tensile test. It was demonstrated that inertia effectively introduces a length scale so that for fixed material properties and a fixed imposed strain rate, specimen ductility is a function of specimen size. Han and Tvergaard (1995) revisited the findings in (Knoche and Needleman, 1993) and confirmed by FE simulations that the effect of inertia delays the onset of necking in plane strain tensile test specimens. The numerical simulations of Hu and Daehn (1996) on rings subjected to rapid expansion indicated that the observed ductility of the expanded rings increases with loading rate, virtually without limits. These

numerical results were consistent with experimental observations and provided further verification of the role played by inertia in retarding flow localization. Additional more recent numerical simulations which emphasize the stabilizing role of inertia in different loading situations and for different types of material behaviors can be found in (Pandolfi et al., 1999; Sørensen and Freund, 2000; Nilsson 2001, Becker, 2002; Tuğcu 2003, Rusinek and Zaera 2007, Rodríguez-Martínez 2013a,b).

Analytical work: Typically this work uses linear stability analysis of a fundamental solution to determine the growth rate of the most preferred perturbations. This analysis yields analytical expressions that reveal the individual influences of the loading and material parameters on the necking process. Fressengeas and Molinari (1985, 1994) studied plastic localization in bars and sheets subjected to rapid extension. Their results explained the increased material ductility at high strain rates and were in qualitative agreement with experimental observations. Similarly, Sørensen and Freund (1998) and Shenoy and Freund (1999) analyzed the stability of a rectangular plate strained under plane strain tension and also showed that inertia tends to slow down the perturbation growth. More recent publications, Molinari and co-workers developed the analysis for the rapid expansion of tubes (Mercier and Molinari 2004) and hemispheres (Mercier et al. 2010) which further justifies the conclusion that inertia is a stabilizing factor which delays flow localization (irrespective of the loading configuration addressed). Rodríguez-Martínez et al. (2013a,b) re-examined the rapid axial stretching of ductile rods and showed that at sufficiently high strain rates, inertia dominates other effects and completely controls the onset of necking. This conclusion was derived by analyzing the stability of a 1D model proposed by Zhou et al. (2006) which incorporated axial inertia.

However, like other analysis of 1D structural elements subjected to uniaxial extension (Vadillo et al. 2012, Rodríguez-Martínez et al. 2013a, Zaera et al. 2013), the model did not include the influence of radial inertia. Consequently, the influence of radial inertia on flow localization in ductile rods subjected to rapid stretching still needs further study.

In this paper, use is made of the theory of a Cosserat curve (e.g. Green et al., 1974a,b and Rubin, 2000) to develop equations for rigid plastic deformations of a straight rod with a deformable circular cross-section. This formulation extends that in (Zhou et al., 2006) by including an averaged effect of the balance of linear momentum associated with radial motion of the cross-section. Examples show the quantitative effect of radial inertia on the stabilization of the localization process.

An outline of the paper is as follows: Section 2 presents the basic equations of a Cosserat rod with specialization for the case of rigid-plastic deformation of a straight rod. Section 3 records the specialized form of the yield strength used in previous analyses and Section 4 develops the equations for linearized deformations superimposed on a nonlinear uniform solution. Section 5 discusses the stability analysis, Section 6 presents results and discussion and Section 7 presents conclusions. Also, the Appendix presents some connections with the three-dimensional theory.

Throughout the text, vectors and second order tensors are denoted by bold symbols, $\mathbf{a} \cdot \mathbf{b}$ denotes the usual dot product between two vectors $\{\mathbf{a}, \mathbf{b}\}$, $\mathbf{a} \otimes \mathbf{b}$ denotes the tensor product between two vectors $\{\mathbf{a},\mathbf{b}\}$, $\mathbf{A} \cdot \mathbf{B} = \mathrm{tr}(\mathbf{A}\mathbf{B}^{\mathrm{T}})$ denotes the inner product between two second order tensors $\{\mathbf{A},\mathbf{B}\}$ and $\mathbf{I}$ is the second order identity tensor.

2. Basic equations of a Cosserat rod

Following the work in Chapter 5 of (Rubin, 2000) the kinematics of a Cosserat rod in its present configuration at time t are specified by

$$\mathbf{x} = \mathbf{x}(\theta^3,t)\ ,\ \ \mathbf{d}_\alpha = \mathbf{d}_\alpha(\theta^3,t)\ , \tag{2.1}$$

where $\mathbf{x}$ locates a material point on the reference curve of the rod and $\mathbf{d}_\alpha$ (α=1,2) are director vectors that characterize the rod's cross-section. Also, θ^3 is a convected coordinate characterizing material points along the reference curve. These quantities can be used to obtain an approximation of the three-dimensional position vector $\mathbf{x}^*$ which locates material points in the rod region

$$\mathbf{x}^* = \mathbf{x}(\theta^3,t) + \theta^\alpha\, \mathbf{d}_\alpha(\theta^3,t)\ \ , \tag{2.2}$$

where θ^α are convected coordinates locating material points in the rod's cross-section and the usual summation convention is used for repeated indices. Here, Greek indices have the range (α=1,2) and Latin indices have the range (i=1,2,3). Also, the director $\mathbf{d}_3$, which is tangent to the rod's reference curve, and the scalar d_{33} are defined by

$$\mathbf{d}_3 = \mathbf{x}_{,3}\ \ ,\ \ d_{33} = \mathbf{d}_3 \bullet \mathbf{d}_3\ \ , \tag{2.3}$$

where a comma denotes partial differentiation with respect to θ^i. Furthermore, the velocity $\mathbf{v}$ and director velocities $\mathbf{w}_i$ are defined by

$$\mathbf{v} = \dot{\mathbf{x}}\ ,\ \mathbf{w}_i = \dot{\mathbf{d}}_i\ \ , \tag{2.4}$$

where a superposed ($\bullet$) denotes material time differentiation holding θ^3 fixed.

The scalar $d^{1/2}$ and reciprocal vectors $\mathbf{d}^i$ of $\mathbf{d}_i$ are defined by

$$d^{1/2} = \mathbf{d}_1\times\mathbf{d}_2 \bullet \mathbf{d}_3 > 0\ ,\ \ \mathbf{d}^1 = d^{-1/2}(\mathbf{d}_2\times\mathbf{d}_3)\ ,\ \ \mathbf{d}^2 = d^{-1/2}(\mathbf{d}_3\times\mathbf{d}_1)\ ,\ \mathbf{d}^3 = d^{-1/2}(\mathbf{d}_1\times\mathbf{d}_2)\ ,$$

$$\mathbf{d}^i \bullet \mathbf{d}_j = \delta^i_j \,, \tag{2.5}$$

where δ^i_j is the Kronecker delta symbol. Moreover, the rate tensor **L**, the rate of deformation tensor **D** and its deviatoric part **D'** are defined by

$$\mathbf{L} = \mathbf{w}_i \otimes \mathbf{d}^i \,, \;\; \mathbf{D} = \frac{1}{2}(\mathbf{L} + \mathbf{L}^T) \,, \;\; \mathbf{D}' = \mathbf{D} - \frac{1}{3}(\mathbf{D} \bullet \mathbf{I})\,\mathbf{I} \;\; . \tag{2.6}$$

In the absence of body forces and tractions on the rod's lateral surface, the balances of linear momentum and director momentum can be written in the forms (Rubin, 2000)

$$m\dot{\mathbf{v}} = \mathbf{t}^3{}_{,3} \,, \;\; m y^{\alpha\beta}\,\dot{\mathbf{w}}_\beta = -\,\mathbf{t}^\alpha + \mathbf{m}^\alpha{}_{,3} \;\; , \tag{2.7}$$

where m is the constant mass per unit length $d\theta^3$, $y^{\alpha\beta} = y^{\beta\alpha}$ are constant director inertia coefficients, $\mathbf{t}^3$ is the force and $\mathbf{m}^\alpha$ are director couples both applied to the end of the rod whose cross-section has a unit outward normal making an acute angle with $\mathbf{d}_3$, and $\mathbf{t}^\alpha$ are intrinsic director couples. These kinetic quantities $\{\mathbf{t}^i, \mathbf{m}^\alpha\}$ need to be specified by constitutive equations. Moreover, the balance of angular momentum requires the tensor **T** be symmetric

$$d_{33}^{1/2}\mathbf{T} = \mathbf{t}^i \otimes \mathbf{d}_i + \mathbf{m}^\alpha \otimes \mathbf{d}_{\alpha,3} = d_{33}^{1/2}\,\mathbf{T}^T \;\; . \tag{2.8}$$

Once constitutive equations are specified for $\{d_{33}^{1/2}\mathbf{T}, \mathbf{m}^\alpha\}$, the expression (2.8) can be used to determine constitutive equations for $\mathbf{t}^i$, such that

$$\mathbf{t}^i = (d_{33}^{1/2}\,\mathbf{T} - \mathbf{m}^\alpha \otimes \mathbf{d}_{\alpha,3})\,\mathbf{d}^i \;\; . \tag{2.9}$$

In this paper, attention is limited to a straight rod with circular cross-section that has radius B in its undeformed reference configuration. For this rod the vectors $\{\mathbf{x}, \mathbf{d}_i\}$ can be specified by

$$\mathbf{x} = z(\theta^3,t)\,\mathbf{e}_3\ ,\ \ \mathbf{d}_\alpha = \phi(\theta^3,t)\,\mathbf{e}_\alpha\ ,\ \ \mathbf{d}_3 = \lambda(\theta^3,t)\,\mathbf{e}_3\ ,\ \ d_{33}^{1/2} = \lambda = \frac{\partial z}{\partial \theta^3}\ , \tag{2.10}$$

where $\mathbf{e}_i$ are fixed rectangular Cartesian base vectors, z denotes the axial position of a material point on the reference curve, ϕ denotes the radial stretch of a material fiber in the rod's cross-section and λ denotes the axial stretch, all in the deformed present configuration. The associated reciprocal vectors are given by

$$\mathbf{d}^\alpha = \frac{1}{\phi}\,\mathbf{e}_\alpha\ ,\ \ \mathbf{d}^3 = \frac{1}{\lambda}\,\mathbf{e}_3\ . \tag{2.11}$$

and the initial (t=0) undeformed configuration is uniform and characterized by

$$z(\theta^3,0) = \theta^3\ ,\ \ \phi(\theta^3,0) = 1\ ,\ \lambda(\theta^3,0) = 1\ . \tag{2.12}$$

Furthermore, the rate of deformation tensor **D** associated with (2.11) is given by

$$\mathbf{D} = \frac{\dot{\phi}}{\phi}\,(\mathbf{e}_1\otimes\mathbf{e}_1+\mathbf{e}_2\otimes\mathbf{e}_2) + \frac{\dot{\lambda}}{\lambda}\,(\mathbf{e}_3\otimes\mathbf{e}_3)\ \ . \tag{2.13}$$

Now, for isochoric motion

$$\lambda\phi^2 = 1\ ,\ \ \mathbf{D}\bullet\mathbf{I} = 2\,\frac{\dot{\phi}}{\phi} + \frac{\dot{\lambda}}{\lambda} = 0\ \ , \tag{2.14}$$

so that

$$\mathbf{D} = \mathbf{D}' = \frac{\dot{\phi}}{\phi}\,(\mathbf{e}_1\otimes\mathbf{e}_1+\mathbf{e}_2\otimes\mathbf{e}_2 - 2\,\mathbf{e}_3\otimes\mathbf{e}_3)\ \ . \tag{2.15}$$

In the Appendix it is shown [(A.8) and (A.9)] that the average area of the rod's deformed cross-section is given by

$$a = \phi^2(\pi B^2)\ \ ,\ d_{33}^{1/2}\,a = \lambda\phi^2(\pi B^2)\ . \tag{2.16}$$

Consequently, with the help of (A.7) the quantity $d_{33}^{1/2}\mathbf{T}$ in (2.8) can be expressed in terms of the average Cauchy stress $\mathbf{T}^*_{avg}$, such that

$$d_{33}^{1/2}\mathbf{T} = d_{33}^{1/2}\, a\, \mathbf{T}^{*}_{avg} = (\pi B^2)\, \mathbf{T}^{*}_{avg} \quad , \tag{2.17}$$

where use has been made of the incompressibility condition (2.14). Furthermore, for an incompressible rigid-plastic material the average Cauchy stress can be expressed in the Levy-Mises form

$$\mathbf{T}^{*}_{avg} = -\, p^{*}_{avg}\, \mathbf{I} + \mathbf{T}^{*\prime}_{avg} \,,$$

$$\mathbf{T}^{*\prime}_{avg} = Y \sqrt{\frac{2}{3}} \frac{\mathbf{D}'}{\sqrt{\mathbf{D}' \bullet \mathbf{D}'}} = \frac{Y}{3} \left(\frac{\dot{\phi}}{|\dot{\phi}|}\right) (\mathbf{e}_1 \otimes \mathbf{e}_1 + \mathbf{e}_2 \otimes \mathbf{e}_2 - 2\, \mathbf{e}_3 \otimes \mathbf{e}_3) \,, \tag{2.18}$$

where the pressure p^{*}_{avg} is an arbitrary function of $\{\theta^3, t\}$ and Y is the yield strength in uniaxial stress. Moreover, since the rod remains straight and the deformation is axisymmetric, the director couples $\mathbf{m}^{\alpha}$ are specified to be zero

$$\mathbf{m}^{\alpha} = 0 \quad . \tag{2.19}$$

Next, with the help of (2.9), (2.11), (2.14) and (2.17)-(2.19) it follows that

$$\mathbf{t}^{\alpha} = \frac{\pi B^2}{\phi} \left[- p^{*}_{avg} + \frac{Y}{3} \left(\frac{\dot{\phi}}{|\dot{\phi}|}\right)\right] \mathbf{e}_{\alpha} \,, \quad \mathbf{t}^{3} = -\, \phi^2\, (\pi B^2) \left[p^{*}_{avg} + \frac{2Y}{3} \left(\frac{\dot{\phi}}{|\dot{\phi}|}\right)\right] \mathbf{e}_3 \quad . \tag{2.20}$$

Moreover, it was shown in (A.9) that

$$m = \rho^{*}(\pi B^2) \,, \quad y^{11} = y^{22} = \frac{B^2}{4} \,, \quad y^{12} = 0 \,, \tag{2.21}$$

where ρ^{*} is the constant mass density. Thus, the equations of motion (2.7) yield two scalar equations given by

$$\rho^{*}\, \ddot{z} = -\, [\phi^2 \{ p^{*}_{avg} + \frac{2Y}{3} \left(\frac{\dot{\phi}}{|\dot{\phi}|}\right)\}]_{,3} \,, \quad \rho^{*} y^{11}\, \ddot{\phi} = -\, \frac{1}{\phi} \left[- p^{*}_{avg} + \frac{Y}{3} \left(\frac{\dot{\phi}}{|\dot{\phi}|}\right)\right] . \tag{2.22a,b}$$

Solving (2.22b) for

$$p^{*}_{avg} = \frac{Y}{3}\left(\frac{\dot{\phi}}{|\dot{\phi}|}\right) + \rho^{*} y^{11} \phi \ddot{\phi} \quad , \tag{2.23}$$

differentiating (2.22a) with respect to θ^3 and using (2.10) and (2.14) yields an equation for ϕ of the form

$$\frac{d^2}{dt^2}\left(\frac{1}{\phi^2}\right) = -\left[\phi^2 \frac{Y}{\rho^{*}}\left(\frac{\dot{\phi}}{|\dot{\phi}|}\right) + y^{11}\phi^3 \ddot{\phi}\right]_{,33} . \tag{2.24}$$

Alternatively, using the incompressibility condition (2.14) this equation can be rewritten in terms of the stretch λ to obtain

$$\ddot{\lambda} = \left[\frac{Y}{\rho^{*}\lambda}\left(\frac{\dot{\lambda}}{|\dot{\lambda}|}\right) + \left(\frac{y^{11}}{2}\right)\lambda^{-3}\left(\ddot{\lambda} - \frac{3}{2}\lambda^{-1}\dot{\lambda}^2\right)\right]_{,33} . \tag{2.25}$$

Now, differentiating the balance of linear momentum, equation (9) in (Rodríguez et al. 2013b), with respect to $X=\theta^3$ and using the expressions $A_0=\pi B^2$, $A=A_0/\lambda$, $\sigma=Y$, $\partial v/\partial X=\dot{\lambda}$ it can be shown that the result is identical to (2.25) when radial inertia is neglected ($y^{33}=0$) and the rod is stretching ($\dot{\lambda}>0$).

3. Influence of the multiaxial stress state during necking

The yield strength Y in the above equations represents the average uniaxial stress required to yield the rod in axial extension or compression. However, when the cross-section of the rod is not axially uniform, as in a necked region, the three-dimensional stress state is multiaxial. Following the work in (Bridgman, 1952; Walsh, 1984; Fressengeas and Molinari, 1985, Zhou et al. 2006) the main effect of this multiaxial stress state can be modeled by specifying Y in the form

$$Y = Y_0 \left(1 + \frac{1}{\theta}\right) \ln(1+\theta) \,, \quad \theta = \frac{1}{2}\, b\, \frac{\partial^2 b}{\partial z^2} = \frac{1}{2}\, b\, \lambda^{-1}\, [\lambda^{-1} b_{,3}]_{,3} \,, \tag{3.1}$$

where b is the current radius of the rod

$$b = \phi B = \lambda^{-1/2} B \,. \tag{3.2}$$

This form of the yield strength is an essential feature of the model (Zhou et al. 2006, Rodríguez et al. 2013a) used to determine the critical growth rate of the most unstable perturbation.

4. Linerized deformation superimposed on a nonlinear uniform solution

For this solution is it assumed that the rod is stretching uniformly with $\dot{\lambda} > 0$ and λ being independent of space so that (2.25) yields

$$\frac{\partial^2\lambda}{\partial t^2} = [\lambda^{-1}(\frac{Y}{\rho^*}) + (\frac{y^{11}}{2})\lambda^{-3}\{\frac{\partial^2\lambda}{\partial t^2} - \frac{3}{2}\lambda^{-1}(\frac{\partial\lambda}{\partial t})^2\}]_{,33} . \tag{4.1}$$

Using (3.1) and (3.2) it follows that a solution of (4.1) which is uniform in space is given by

$$\lambda = \lambda_0[1+(\frac{\dot{\varepsilon}_0}{\lambda_0})t] \quad , \ \lambda(0) = \lambda_0 = \phi_0^{-2} \ , \ \dot{\lambda}(0) = \dot{\varepsilon}_0 \ , \tag{4.2}$$

where λ_0 is the initial axial stretch, ϕ_0 is the initial radial stretch, and $\dot{\varepsilon}_0$ is the initial rate of axial stretch. Motivated by the form of this solution it is convenient to introduce the normalized variables

$$T = (\frac{\dot{\varepsilon}_0}{\lambda_0})t \ , \ Z = \frac{\theta^3}{B} \ . \tag{4.3}$$

Then, taking $\lambda=\lambda(Z,T)$ equation (4.1) can be rewritten in the form

$$\frac{\partial^2\lambda}{\partial T^2} = \frac{\partial^2}{\partial Z^2}[\lambda^{-1}(\frac{Y\lambda_0^2}{\rho^* B^2\dot{\varepsilon}_0^2}) + (\frac{y^{11}}{2B^2})\lambda^{-3}\{\frac{\partial^2\lambda}{\partial T^2} - \frac{3}{2}\lambda^{-1}(\frac{\partial\lambda}{\partial T})^2\}] \ , \tag{4.4}$$

where Y is given by (3.1).

Next, consider a perturbation of the solution (4.2) given by

$$\lambda = \lambda_0(1+T) + \eta \ , \ \eta = \eta(Z,T) \ . \tag{4.5}$$

Then, neglecting quadratic terms in η and its derivatives and using the approximations

$$\lambda = \lambda_0(1+T)[1+\frac{\eta}{\lambda_0}(1+T)^{-1}] \ , \ \lambda^{-1} = \lambda_0^{-1}(1+T)^{-1}[1-\frac{\eta}{\lambda_0}(1+T)^{-1}] \ , \tag{4.6}$$

the expressions (3.1) and (3.2) reduce to

$$\theta = -\frac{1}{4}\lambda_0^{-4}(1+T)^{-4}\ \frac{\partial^2\eta}{\partial Z^2}\ ,\ Y = Y_0(1+\frac{1}{2}\theta) = Y_0[1-\frac{1}{8\lambda_0^4}(1+T)^{-4}\ \frac{\partial^2\eta}{\partial Z^2}]\ , \qquad (4.7)$$

and equation (4.4) can be approximated by

$$\frac{\partial^2\eta}{\partial T^2} - (\frac{y^{11}}{2B^2\lambda_0^3})(1+T)^{-3}\ \frac{\partial^4\eta}{\partial T^2\partial Z^2} + 3\ (\frac{y^{11}}{2B^2\lambda_0^3})\ (1+T)^{-4}\ \frac{\partial^3\eta}{\partial T\partial Z^2}$$

$$+\ [(\frac{Y_0}{\rho^* B^2\dot{\varepsilon}_0^2})\ (1+T)^{-2} -\ 6\ (\frac{y^{11}}{2B^2\lambda_0^3})\ \lambda_0^{-2}(1+T)^{-5}]\ \frac{\partial^2\eta}{\partial Z^2}$$

$$+\frac{1}{8}\ (\frac{Y_0}{\rho^* B^2\dot{\varepsilon}_0^2})\lambda_0^{-3}\ (1+T)^{-5}\ \frac{\partial^4\eta}{\partial Z^4} = 0\ . \qquad (4.8)$$

5. Stability analysis

In order to analyze the stability of the solution (4.5) consider a perturbation of the form

$$\eta = g(T)\cos(KZ) \ , \tag{5.1}$$

where K is a normalized wavenumber. Substituting this function into (4.8) yields an equation for g(T) of the form

$$[1 + (\frac{y^{11}}{2B^2\lambda_0^3})K^2(1+T)^{-3}]\frac{d^2g}{dT^2} - 3(\frac{y^{11}}{2B^2\lambda_0^3})K^2(1+T)^{-4}\frac{dg}{dT} - K^2[(\frac{Y_0}{\rho^* B^2 \dot{\varepsilon}_0^2})(1+T)^{-2}$$

$$- 6(\frac{y^{11}}{2B^2\lambda_0^3})\lambda_0^{-2}(1+T)^{-5} - \frac{1}{8}(\frac{Y_0}{\rho^* B^2 \dot{\varepsilon}_0^2})\lambda_0^{-3}(1+T)^{-5}K^2]\, g = 0 \ . \tag{5.2}$$

Short time solution

For the short time solution the term (1+T) is approximated by unity to obtain the equation

$$(1+a_1K^2)\frac{d^2g}{dT^2} - 3a_1K^2\frac{dg}{dT} - K^2[\frac{1}{a_0}(1 - \frac{1}{8\lambda_0^3}K^2) - (\frac{6}{\lambda_0^2})a_1]\, g = 0 \quad , \tag{5.3}$$

where the normalized axial loading rate a_0 and the normalized radial inertia a_1 are defined by

$$a_0 = \frac{\rho^* B^2 \dot{\varepsilon}_0^2}{Y_0 \phi_0^4} \ , \quad a_1 = \frac{y^{11}}{2B^2\lambda_0^3} = \frac{1}{8\lambda_0^3} \ . \tag{5.4}$$

and where use was made of (2.21). The reciprocal of a_0 was referred to in (Knoche and Needleman, 1993; Mercier and Molinari, 2003, Mercier and Molinari 2004; Zhou et al., 2006; Vadillo et al., 2012) as an axial inertia parameter. Here, it is referred to as a

loading rate parameter since for fixed rod geometry and material properties the value of a_0 can be changed by orders of magnitude by specifying different axial extension rates $\dot{\varepsilon}_0$. Moreover, the parameter a_1 controls the influence of radial inertia and is positive ($a_1 > 0$) when radial inertia is included and is zero ($a_1 = 0$) when radial inertia is excluded.

Next, the solution of (5.3) is taken in the form

$$g = \exp(\omega T) \ , \tag{5.5}$$

where ω is the normalized growth rate of perturbations. Then, substitution of (5.5) into (5.3) yields the dispersion relationship

$$(1+a_1K^2)\omega^2 - 3a_1K^2\omega - K^2[\frac{1}{a_0}(1 - \frac{1}{8\lambda_0^3}K^2) - (\frac{6}{\lambda_0^2})\,a_1] = 0 \ . \tag{5.6}$$

The critical values $\{\omega_{cr}, K_{cr}\}$ of $\{\omega,K\}$ can be determined by solving

$$\frac{d\omega}{dK} = 0 \ , \tag{5.7}$$

to deduce that

$$\omega_{cr} = \frac{3}{2}\,[1 + \{1 + \frac{4}{9a_0a_1}\,[1 - (\frac{6}{\lambda_0^2})\,a_1 - \frac{1}{4\lambda_0^3}\,K_{cr}^2]\}^{1/2}] \ ,$$

$$\text{with } 0 \le K_{cr} \le 2\lambda_0^{3/2}(1 - \frac{6a_1}{\lambda_0^2})^{1/2} \ \text{ and } \ \frac{6a_1}{\lambda_0^2} \le 1 \ . \tag{5.8}$$

Then, setting $\omega = \omega_{cr}$ and $K = K_{cr}$ in (5.6) and using (5.8) yields an equation for K_{cr} which needs to be solved numerically. Moreover, with the help of (5.1) the critical wavelength L_{cr} associated with this critical wavenumber is given by

$$K_{cr}(\frac{L_{cr}}{B}) = 2\pi \ , \ L_{cr} = (\frac{2\pi}{K_{cr}})B \ . \tag{5.9}$$

It has been shown in (Rodríguez-Martínez et al., 2013b) that L_{cr} is a good estimate of the length of the fragments caused by necking of a rapidly elongating rod.

For the examples considered later the value of a_0 remains less than about 10^{-2} (large strain rates) so the dispersion relation (5.6) can be approximated by

$$\omega^2 = \frac{K^2}{a_0(1+a_1K^2)}(1 - \frac{1}{8\lambda_0^3}K^2) \quad \text{for} \ \ 0 \le \frac{1}{8\lambda_0^3}K^2 \le 1 \ , \tag{5.10}$$

which yields the critical values

$$\omega_{cr} = [\frac{K_{cr}^2}{a_0(1+a_1K_{cr}^2)}(1 - \frac{1}{8\lambda_0^3}K_{cr}^2)]^{1/2} \ , \ K_{cr} = [\frac{1}{a_1}\{-1 + (1 + 8a_1\lambda_0^3)^{1/2}\}]^{1/2} \ . \tag{5.11}$$

The results in this section can be compared with those in (Rodríguez-Martínez et al., 2013b) by noting that the parameters there can be related to the parameters here using the expressions

$$r_0 \to B \ , \ \chi_m \to 0 \ , \ \chi_n \to 0 \ , \ \Psi \to Y_0 \ , \ \dot{\bar{\varepsilon}}_1 \to \dot{\bar{\varepsilon}}_0 \ ,$$

$$\Lambda \to \frac{1}{\lambda_0} \ , \ \bar{\eta} \to \omega \ , \ \bar{\xi} \to K \ , \ \bar{L}^2 \to \frac{Y_0}{\rho^* B^2 \dot{\bar{\varepsilon}}_0^2} \ , \tag{5.12}$$

where the effects of hardening due to strain and strain rate have been neglected. Then, the equation (16) in (Rodríguez-Martínez et al., 2013b) can be written in the form

$$\omega^2 + \omega - \frac{K^2}{a_0}(1 - \frac{1}{8\lambda_0^3}K^2) = 0 \ . \tag{5.13}$$

This equation can be compared with (5.6) when radial inertia is neglected ($a_1 = 0$)

$$\omega^2 = \frac{K^2}{a_0}\left(1 - \frac{1}{8\lambda_0^3}K^2\right) \ , \tag{5.14}$$

which yields the critical values

$$K_{cr} = 2\lambda_0^{3/2} \ , \ L_{cr} = (\pi\phi_0)B \ , \ \omega_{cr} = \left(\frac{2}{a_0}\right)^{1/2}\lambda_0^{3/2} \ . \tag{5.15}$$

The differences between (5.13) and (5.14) are most likely due to the fact that here perturbations are taken relative to the exact nonlinear uniform solution (4.2). However, as mentioned previously, for the small values of a_0 associated with the example problems discussed later the linear term in ω in (5.13) can be neglected so (5.13) and (5.14) yield nearly the same results.

6. Results and discussion

The objective of this section is to consider examples that reveal the quantitative influence of radial inertia on flow localization in ductile rods subjected to dynamic extension. Rodríguez-Martínez et al. (2013b) have suggested that since ω is always greater than 12 for the values of a_0 of interest (see Fig. 1) it is reasonable to assume that the onset of necking occurs immediately with the initial value of λ_0 being unity

$$\lambda_0 = 1 \, . \tag{6.1}$$

More specifically, the full equations (5.6) and (5.8) are solved to determine the growth rate ω of perturbations with wavenumber K. These equations include radial inertia when a_1 is given by (5.4) and they exclude radial inertia when $a_1 = 0$. Figure 1 shows plots of ω versus K for different values of the axial inertia parameter a_0. The shapes of these curves are typical of those predicted by this type of stability analysis (Mercier and Molinari 2003, Mercier and Molinari 2004, Zhou et al. 2006, Vadillo et al. 2012, Rodríguez-Martínez 2013b). More specifically, sufficiently short and large wavelengths are stabilized, with the maximum growth rate $\omega = \omega_{cr}$ occurring when $K = K_{cr}$. As reported in (Mercier and Molinari 2003, Mercier and Molinari 2004, Zhou et al. 2006, Vadillo et al. 2012, Rodríguez-Martínez 2013a) the critical value K_{cr} determines the spacing between localization points in multiple necking processes.

From Figure 1 it is observed that the growth rate of the perturbation is larger for the smaller value of a_0, which corresponds to a small axial strain rate, and is smaller for the larger value of a_0, which corresponds to a large axial strain rate. Radial inertia does not change the range of wavenumbers which grow. This range is determined mainly by the

combined effect of axial inertia and stress multiaxiality effects (Fressengeas and Molinari, 1994). As expected, radial inertia tends to reduce the maximum rate of growth of perturbations, with a larger influence on short wavelengths. Figure 1 also shows that radial inertia tends to increase the critical wavelength, which is consistent with the approximate analytical result (5.11).

In order to study the quantitative influence of radial inertia it is convenient to define the parameters $\{\bar{\omega}_{cr}, \bar{K}_{cr}\}$ by

$$\bar{\omega}_{cr} = \frac{\omega_{cr}(NR)}{\omega_{cr}(R)} \ , \quad \bar{K}_{cr} = \frac{K_{cr}(NR)}{K_{cr}(R)} \ , \tag{6.2}$$

where $\{\omega_{cr}(R), K_{cr}(R)\}$ and $\{\omega_{cr}(NR), K_{cr}(NR)\}$ are the critical values $\{\omega_{cr}, K_{cr}\}$, respectively, including (R with $a_1 > 0$) and excluding (NR with $a_1 = 0$) the effect of radial inertia. Figure 2 shows the plot of $\bar{\omega}_{cr}$ versus K for two values of the loading rate parameter a_0. From this figure it can be observed that the influence of radial inertia on the growth rate is a nonlinear function of the wavenumber K. Mercier and Molinari (2003, 2004) indicated that axial inertia has a greater stabilizing effect on long wavelengths. In contrast, from Fig. 2 it can be seen that radial inertia has a greater stabilizing effect on short wavelengths, which is in addition to the stabilization of short wavelengths due to the multiaxial stress state in the necking region. Moreover, for the smaller strain rate (the smallest value of a_0) radial inertia decreases the rate of growth of the larger wavenumbers by about 40%.

Next, attention is focused on the influence of radial inertia on the critical perturbation growth rate ω_{cr} and on the critical wavenumber K_{cr}. Figures 3 show: (a) the critical growth rate ω_{cr} and (b) the critical wavenumber K_{cr} versus a_0 including (R) and excluding (NR) the effect of radial inertia. From Figure 3a it can be seen that the growth rate increases with decreasing loading rate (smaller values of a_0), with the influence of radial inertia becoming smaller with increasing loading rate (large values of a_0).

In the absence of radial inertia (5.15) predicts that the critical wavenumber K_{cr} is constant. This constant value of K_{cr} suggests that the number of necks formed (neck spacing) in an axially stretched rod is independent of the loading rate. However, the numerical observations reported for rate-independent materials in (Rodríguez-Martínez et al., 2013a,b) indicate that the neck spacing increases as the loading rate decreases (decreasing values of a_0). This observation would suggest that K_{cr} decreases with decreasing values of a_0. Figure 3b shows the dependence of the critical wavenumber K_{cr} on the value of a_0 predicted by the constant value (5.15) when radial inertia is neglected and by the numerical solution of the full equation (5.8) when radial inertia is included. The small drop in K_{cr} shown in Figure 3b for the solution with radial inertia is consistent with the numerical results in (Rodríguez-Martínez et al., 2013a,b) however it is inconsistent with the approximate value (5.15) for large a_0. This partially quantifies the error in the approximate values (5.15).

Figure 4 plots the relative quantities $\{\bar{\omega}_{cr}, \bar{K}_{cr}\}$ defined in (6.2) versus a_0. From this figure it can be seen that neglecting radial inertia causes an increase in both the growth

rate ω_{cr} and the wavenumber K_{cr}, with larger increases for slower loading rates (smaller values of a_0). Specifically, for the smallest value $a_0 = 10^{-6}$ neglecting radial inertia increases ω_{cr} by about 21% and increases K_{cr} by about 10%. Whereas, for the largest value $a_0 = 10^{-2}$ neglecting radial inertia increases ω_{cr} by about 17% and increases K_{cr} by about 8%. Unlimited increase in extension rate (increase in a_0) will cause the effect of radial inertia to become negligible.

7. Conclusions

The effect of radial inertia on flow localization in ductile rods subjected to rapid extension has been examined using linear stability analysis of an exact solution for nonlinear uniform extension of a rigid-plastic straight Cosserat rod. This model generalizes the original formulation derived by Zhou et al. (2006) by taking into account the radial stretching experienced by the rod. The main results of this investigation can be summarized as:

- Radial inertia tends to stabilize the localization process by slowing down the rate of growth of perturbations.
- The stabilizing effect of radial inertia becomes more significant as the rate of extension decreases.
- Radial inertia decreases both the critical growth rate of the perturbation and the critical wavenumber, with a larger effect for smaller rates of extension.
- In contrast with axial inertia, which has a greater stabilizing effect on long wavelengths (Mercier and Molinari, 2003, 2004), radial inertia has a greater stabilizing effect on short wavelengths.

Acknowledgements

This research was partially supported by MB Rubin's Gerard Swope Chair in Mechanics. J. A. Rodríguez-Martínez is indebted to the Ministerio de Ciencia e Innovación de España (Project DPI/2011-24068) for the financial support. J. A. Rodríguez-Martínez expresses sincere gratitude to G. Vadillo, J. Fernández-Sáez, R. Zaera and A. Molinari for helpful discussions on flow localization in ductile materials subjected to high strain rates.

References

Altynova, M., Hu, X., Daehn, G.S., 1996. Increased ductility in high velocity electromagnetic ring expansion. Metallurgical Transactions A 27, 1837-1844.

Becker, R., 2002. Ring fragmentation predictions using the Gurson model with material stability conditions as failure criterion. Int. J. Solids Struct. 39, 3555-3580.

Bridgman, P.W., 1952. Studies in large plastic flow and fracture, with special emphasis on the effects of hydrostatic pressure, vol. 1, McGraw-Hill Book Company Inc, New York, pp. 9–37.

Considère, A. G., 1885. L'emploi du fer de l'acier dans les constructions. Ann. Ponts et Chausses 9, 574-575.

Fressengeas, C., Molinari, A., 1985. Inertia and thermal effects on the localization of plastic flow. Acta Metall. 33, 387-396.

Fressengeas, C., Molinari, A., 1994. Fragmentation of rapidly stretching sheets. Eur. J. Mech. A/Solids 13, 251-268.

Fyfe, I. M., Rajendran, A. M., 1980. Dynamic Pre-Strain and Inertia Effects on the Fracture of Metals. Journal of the Mechanics and Physics of Solids, 28, 17-26.

Goto, D., Becker, R., Orzechowski, T., Springer, H., Sunwoo, A., Syn, C., 2008. Investigation of the fracture and fragmentation of explosively driven rings and cylinders. International Journal of Impact Engineering 35, 1547–1556.

Gourdin, W.H., 1989. Analysis and assessment of electromagnetic ring expansion as a high-strain-rate test. Journal of Applied Physics 65, 411-422.

Grady, D.E., 1982. Local inertia effects in dynamic fragmentation. J. Appl. Phys. 68, 322-325.

Grady, D.E., Benson, D.A., 1983. Fragmentation of metal rings by electromagnetic loading. Experimental Mechanics 12, 393-400.

Grady, D.E., Olsen, M.L., 2003. A statistics and energy based theory of dynamic fragmentation. International Journal of Impact Engineering 29, 293-306.

Green A.E., Naghdi P.M., Wenner M.L., 1974a. On the theory of rods – Part I: Derivations from the three-dimensional equations. Proc. Royal Soc. London A337, 451-483.

Green A.E., Naghdi P.M., Wenner M.L., 1974b. On the theory of rods – Part II: Developments by direct approach. Proc. Royal Soc. London A337, 485-507.

Han, J.B., Tvergaard, V., 1995. Effect of inertia on the necking behaviour of ring specimens under rapid axial expansion. European Journal of Mechanics A/Solids 14, 287-307.

Hiroe, T., Fujiwara, K., Hata, H., Takahashi, H., 2008. Deformation and fragmentation behaviour of exploded metal cylinders and the effects of wall materials,

configuration, explosive energy and initiated locations. International Journal of Impact Engineering 35, 1578–586.

Hu, X., Daehn, G.S., 1996. Effect of velocity on flow localization in tension. Acta Materialia 44, 1021–1033.

Knoche, P., Needleman, A., 1993. The effect of size on the ductility of dynamically loaded tensile bars. European Journal of Mechanics A/ Solids 12, 586-601.

Janiszewski, J., 2012. Ductility of selected metals under electromagnetic ring test loading conditions. International Journal of Solids and Structures 49, 1001-1008.

Juanicotena, A., 1998. Etude théorique et expérimentale du comportement viscoplastique des matériaux aux grandes déformations et grandes vitesses de déformation. Ph.D. thesis, Université de Metz and Commissariat à l'Energie Atomique.

Mercier, S., Molinari, A., 2004. Analysis of multiple necking in rings under rapid radial expansion. Int. J. Impact Eng. 4, 403-419.

Mercier, S., Granier, N., Molinari, A., Llorca, F., Buy, F., 2010. Multiple necking during the dynamic expansion of hemispherical metallic shells, from experiments to modelling. J. Mech. Phys. Solids 58, 955–982.

Nilsson, K., 2001. Effects of inertia on dynamic neck formation in tensile bars. European Journal of Mechanics A/Solids. 20, 713-729.

Pandolfi, A., Krysl, P., Ortiz, M., 1999. Finite element simulation of ring expansion and fragmentation: the capturing of length and time scales through cohesive models of fracture. Int. J. Fract. 95, 297.

Rajendran, A.M., Fyfe, I.M., 1982. Inertia effects on the ductile failure of thin rings. J. Appl. Mech. 49, 31-36.

Rodríguez-Martínez, J.A., Vadillo, G., Zaera, R., Fernández-Sáez, J., 2013a. On the complete extinction of selected imperfection wavelengths in dynamically expanded ductile rings. Mech. Mater. 60, 107-120.

Rodríguez-Martínez, J.A., Vadillo, G., Fernández-Sáez, J., Molinari, A., 2013b. Identification of the critical wavelength responsible for the fragmentation of ductile rings expanding at very high strain rates. Journal of the Mechanics and Physics of Solids. 61, 1357-1376.

Rubin M.B., 2000. *Cosserat Theories: Shells, Rods and Points*. Solid Mechanics and its Applications, Vol. 79, Kluwer, The Netherlands.

Rusinek, A., Zaera, R., 2007. Finite element simulation of steel ring fragmentation under radial expansion. Int. J. Impact Eng. 34, 799–822.

Sørensen, N.J., Freund, L.B., 1998. Dynamic bifurcation during high-rate planar extension of a thin rectangular block. Eur. J. Mech. A/Solids 17, 709-724.

Sørensen, N.J., Freund, L.B., 2000. Unstable neck formation in a ductile ring subjected to impulsive radial loading. Int. J. Solids Struct. 37, 2265-2283.

Shenoy, V.B., Freund, L.B., 1999. Necking bifurcations during high strain rate extension. J. Mech. Phys. Solids 47, 2209-2233.

Tuğcu, P., 2003. Instability and ductile failure of thin cylindrical tubes under internal pressure impact. International Journal of Impact Engineering 28, 183-205.

Vadillo, G., Rodríguez-Martínez, J.A., Fernández-Sáez, J., 2012. On the interplay between strain rate and strain rate sensitivity on flow localization in the dynamic expansion of ductile rings. International Journal of Solids and Structures 49, 481–491.

Walsh, J. M., 1984. Plastic instability and particulation in stretching metals jets. Journal of Applied Physics 56, 1997–2006.

Zaera R., Rodríguez-Martínez J. A., Vadillo G., Fernández-Sáez J., 2013. Dynamic necking in materials with strain induced martensitic transformation. Submitted for publication to the Journal of the Mechanics and Physics of Solids.

Zhang, H., Ravi-Chandar, K., 2006. On the dynamics of necking and fragmentation – I. Real-time and post-mortem observations in Al 6061-O. International Journal of Fracture 142, 183-217.

Zhou, F., Molinari, J.F., Ramesh, K.T., 2006. An elasto-visco-plastic analysis of ductile expanding ring. Int. J. Impact Eng. 33, 880–891.

Appendix: Some connections with the three-dimensional theory

From the point of view of the three-dimensional theory the kinematic approximation (2.2) can be used to obtain the covariant base vectors $\mathbf{g}_i$ and the scalar $g^{1/2}$ by

$$\mathbf{g}_\alpha = \mathbf{x}^*{}_{,\alpha} = \mathbf{d}_\alpha \, , \;\; \mathbf{g}_3 = \mathbf{x}^*{}_{,3} = \mathbf{d}_3 + \theta^\alpha \mathbf{d}_{\alpha,3} \, , \;\; g^{1/2} = \mathbf{g}_1 \times \mathbf{g}_2 \bullet \mathbf{g}_3 > 0 \, , \tag{A.1}$$

and the reciprocal vectors $\mathbf{g}^i$ are defined by

$$\mathbf{g}^1 = g^{-1/2}(\mathbf{g}_2 \times \mathbf{g}_3) \, , \;\; \mathbf{g}^2 = g^{-1/2}(\mathbf{g}_3 \times \mathbf{g}_1) \, , \; \mathbf{g}^3 = g^{-1/2}(\mathbf{g}_1 \times \mathbf{g}_2) \, , \;\; \mathbf{g}^i \bullet \mathbf{g}_j = \delta^i{}_j \, . \tag{A.2}$$

Moreover, the vectors $\mathbf{t}^{*i}$ are defined in terms of the three-dimensional Cauchy stress $\mathbf{T}^*$ by

$$\mathbf{t}^{*i} = g^{1/2} \mathbf{T}^* \mathbf{g}^i \, . \tag{A.3}$$

Then, the mass quantity m, the director inertia coefficients $y^{\alpha\beta}$ and the kinetic quantities $\mathbf{t}^i$ and $\mathbf{m}^\alpha$ can be defined by the integrals

$$m = \int_A \rho^* g^{1/2} d\theta^1 d\theta^2 \;\; , \;\; m y^{\alpha\beta} = \int_A \theta^\alpha \theta^\beta \, \rho^* g^{1/2} d\theta^1 d\theta^2 \, ,$$

$$\mathbf{t}^i = \int_A \mathbf{t}^{*i} \, d\theta^1 d\theta^2 \, , \; \mathbf{m}^\alpha = \int_A \theta^\alpha \, \mathbf{t}^{*3} \, d\theta^1 d\theta^2 \;\; , \tag{A.4}$$

where ρ^* is the mass density per unit current volume and A characterizes the region of the cross-section in terms of the convected coordinates θ^α. Also, in writing the balance laws (2.7) the convected coordinates θ^α have been specified so that

$$\int_A \theta^\alpha \, \rho^* g^{1/2} d\theta^1 d\theta^2 \; = 0 \, . \tag{A.5}$$

Next, substituting (A.4) into (2.8) and using the fact that

$$\mathbf{g}^i \otimes \mathbf{g}_i = \mathbf{I} \;\; , \tag{A.6}$$

it follows with the help of (A.1) that

$$d_{33}^{1/2}\mathbf{T} = \int_A [\mathbf{t}^{*\alpha}\otimes\mathbf{d}_\alpha + \mathbf{t}^{*3}\otimes(\mathbf{d}_3+\theta^\alpha\mathbf{d}_{\alpha,3})]\, d\theta^1 d\theta^2 = \int_A \mathbf{T}^*\, g^{1/2} d\theta^1 d\theta^2 \,. \qquad (A.7)$$

Now, it is convenient to define the scalar a by the expression

$$d_{33}^{1/2}\, a = \int_A g^{1/2} d\theta^1 d\theta^2 \,. \qquad (A.8)$$

Since $\{d_{33}^{1/2}\, d\theta^3\}$ represents the element of arc-length of deformed reference curve, the scalar a represents the average area of the rod's deformed cross-section

Using the kinematics (2.10) for a straight rod and the condition of incompressibility (2.14) it follows that $g^{1/2} = \lambda\phi^2 = 1$. Moreover, considering a circular rod with reference radius B and transforming the rectangular Cartesian convected coordinates θ^α to convected polar coordinates $\{R,\theta\}$ it can be shown that

$$\theta^1 = R\cos\theta \,,\ \theta^2 = R\sin\theta \,,$$

$$d_{33}^{1/2}\, a = \lambda\, a = \int_0^{2\pi}\int_0^B \lambda\phi^2\ R dR d\theta = \pi B^2 \,,\ a = \phi^2(\pi B^2) \,,$$

$$m = \int_0^{2\pi}\int_0^B \rho^*\lambda\phi^2\ R dR d\theta = \rho^*(\pi B^2) \,,$$

$$my^{11} = \int_0^{2\pi}\int_0^B \rho^*\lambda\phi^2 R^2\cos^2\theta\ R dR d\theta = m\frac{B^2}{4} \,,$$

$$my^{22} = \int_0^{2\pi}\int_0^B \rho^*\lambda\phi^2 R^2\sin^2\theta\ R dR d\theta = m\frac{B^2}{4} \,. \qquad (A.9)$$

In these expressions it has been assumed that the density ρ^* is constant and uniform.

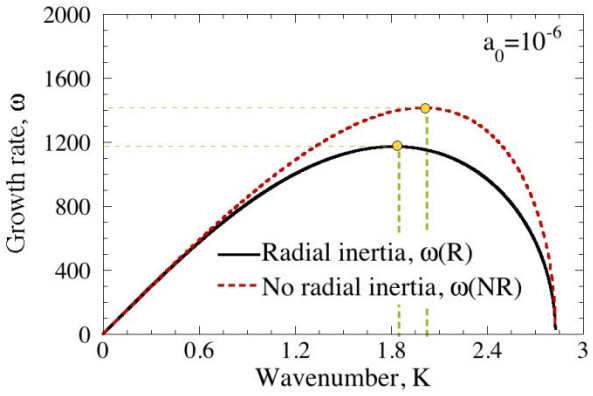

(a)

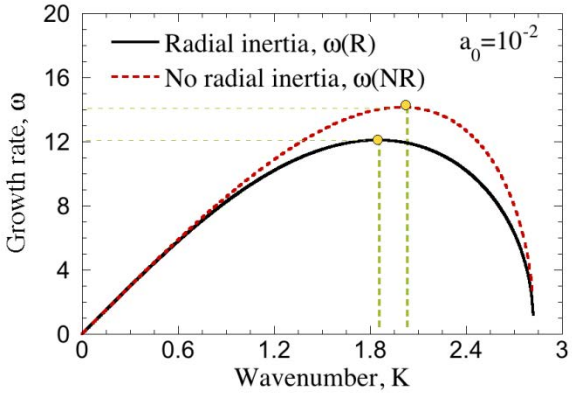

(b)

Fig. 1 Perturbation growth rate ω versus wavenumber K including (R) and excluding (NR) radial inertia for two values of the axial loading rate a_0.

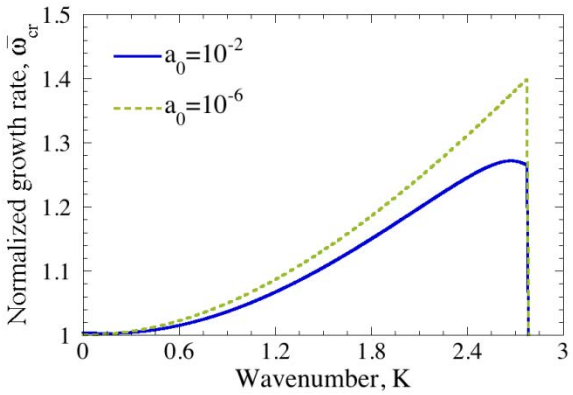

Fig. 2 Ratio of the critical growth rate $\bar{\omega}_{cr}$ of the predictions with no radial inertia relative to those with radial inertia versus the wavenumber K for two values of the axial loading rate a_0.

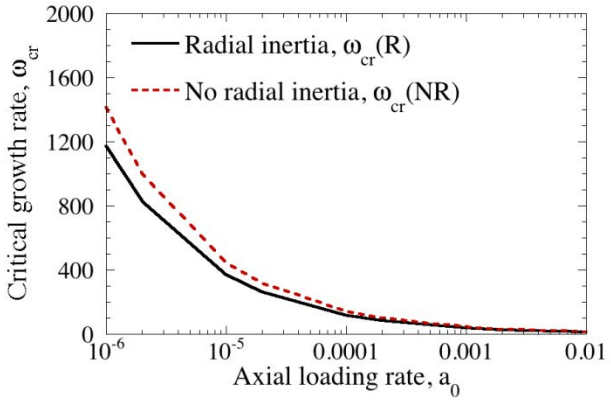

(a)

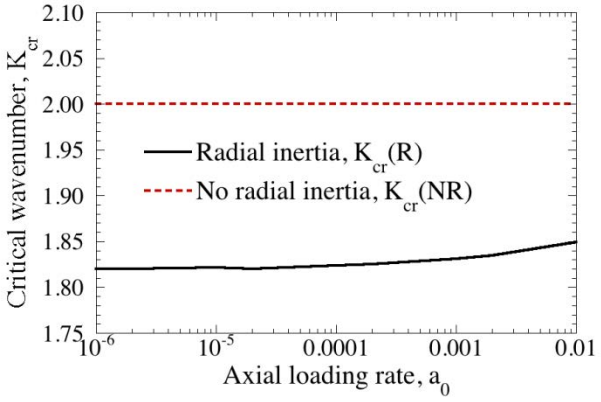

(b)

Fig. 3 (a) Critical perturbation growth rate ω_{cr} and (b) critical wavenumber K_{cr}, both versus the axial loading rate a_0 including (R) and excluding (NR) the effect of radial inertia.

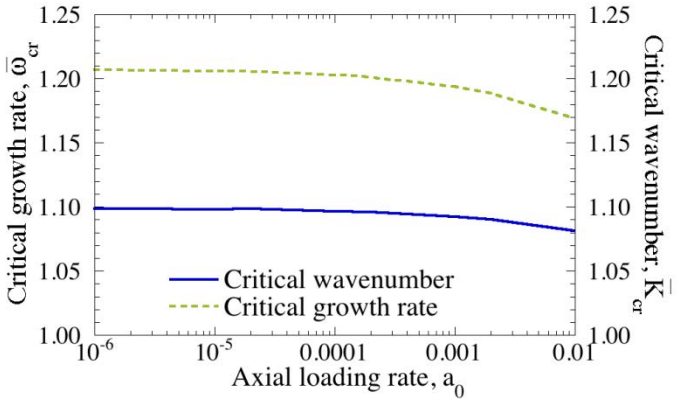

Fig. 4 The normalized critical perturbation growth rate $\bar{\omega}_{cr}$ and the normalized critical wavenumber K_{cr} versus the axial loading rate a_0.